Melting curve of tantalum from first principles

S. Taioli,[1] C. Cazorla,[2,3] M. J. Gillan,[2,3] and D. Alfè[1,2,3]
[1]*Department of Earth Sciences, University College London, Gower Street, London WC1E 6BT, United Kingdom*
[2]*Department of Physics and Astronomy, University College London, Gower Street, London WC1E 6BT, United Kingdom*
[3]*London Centre for Nanotechnology, University College London, Gower Street, London WC1E 6BT, United Kingdom*
(Received 2 February 2007; revised manuscript received 28 March 2007; published 5 June 2007)

We report on the first-principles calculation of the melting curve of Ta in the pressure range 0–300 GPa. The calculations have been performed using density functional theory (DFT) with generalized gradient corrections and the projector augmented wave method. The melting curve has been evaluated using the method of the coexistence of phases, with the help of an auxiliary reference potential. The melting curve obtained with the reference potential has then been corrected using free energy differences between the DFT and the reference potential, so as to obtain the DFT melting curve. The results are in good agreement with diamond anvil cell experiments at low pressure, but they rapidly diverge from these as pressure is increased, and agree well with shock-wave experiments at high pressure. A general description of the lattice dynamics and thermal properties of body-centered cubic tantalum using DFT is also presented. The equation of state at zero temperature and the phonon dispersion are investigated using both the local density approximation and the generalized gradient approximation (GGA). Good agreement with the zero-temperature equation of state and zero-pressure phonon dispersions is obtained with the GGA. This agreement reinforces the reliability of the calculated melting curve.

DOI: 10.1103/PhysRevB.75.214103 PACS number(s): 61.20.Ja, 71.15.Pd, 71.22.+i, 64.70.Dv

I. INTRODUCTION

A fundamental issue in material physics and geophysics is the understanding of the behavior of metals under extreme conditions. Tantalum is a transition metal with multiphase thermodynamic behavior; the specific crystalline structures are a body-centered cubic[1] (bcc) or α phase, stable even at high pressure of hundreds of GPa in the bulk material, a β phase, stable in deposited thin films up to 1000 K,[2] and an $A15$ structure, which could be energetically competitive with the bcc at a very low pressure regime, whereas face-centered-cubic (fcc) and hexagonal-closed-packed (hcp) phases are not.[3] Furthermore, the bcc crystal structure presents a very high melting point at room pressure at about 3270 K. Due to its chemical stability it is widely used in the microelectronics industry for producing integrated circuits.

In this paper, we are mainly concerned with the thermodynamical properties of Ta as functions of temperature and pressure, and in particular its melting curve.

While a large effort has been made to improve the experimental setup for studying phase transitions at high pressures by the use of shock waves[4,5] and laser-heated diamond-anvil cells (DACs),[6,7] large discrepancies between these experiments still exist, in particular about melting curves. Although DAC experiments are only available up to relatively low pressures of about 100 GPa, extrapolations from measurements on tantalum and molybdenum to pressures of 300 GPa show a discrepancy between DAC and shock-wave experiments of several thousand degrees.

Calculation of the dependence of the electronic structure and nuclear motion on pressure and temperature is still a challenge for theory, due to the difficulty of taking fully into account the complex many-body interactions between the electrons, and the interplay between electrons and phonons. In the last few years, advances in computer power and development in computation techniques have made it possible to numerically solve many-body problems for a variety of metals, including transition metals,[8,9] under extreme conditions of temperature and pressure. In particular, first-principles thermodynamic quantities, including melting curves, have been calculated using density functional theory (DFT), and although good agreement is present with experiments for materials like Al (Refs. 10–12) and Cu,[11] significant disagreement with DAC experiments has been reported for the melting curves of MgO (Ref. 13) and Fe,[14,15] although in the case of Fe a number of DAC experiments are available with results often in conflict with each other.[16–18]

On the melting of Ta, we mention the early work of Moriarty *et al.*,[3] who employed the so-called generalized pseudopotential theory method and calculated a melting curve that agreed well with the shock datum[5] but was several thousand degrees above the extrapolated DAC measurements.[7] More recent calculations are due to Strachan *et al.*,[19] who calculated the melting curve of Ta using an embedded atom model (EAM), and obtained results not very different from the earlier ones of Moriarty *et al.*[3]

The differences between theoretical results on the melting of transition metals and some DAC experiments are still the subject of discussion.[20] It has been suggested that the shallow slope of the melting curve of bcc metals, compared to that of nearly-free-electron metals like Al, could be due to electronic rearrangements upon melting.

The main aim of this work is to produce the complete melting curve of Ta from first-principles calculations. The results will then be compared with previous molecular dynamics calculations[3,19] and experiments.[4,7]

A number of different approaches have been used in the past to calculate melting curves of materials. One possibility is to use the free energy approach, which consists in evaluating the Gibbs free energies of solid, $G_s(p,T)$, and liquid, $G_l(p,T)$, as functions of pressure and temperature, and then obtaining the melting temperature T_m at each fixed pressure p

by the condition $G_l(p,T)=G_s(p,T)$.[10,11,14,21–23] Another possibility is to use the so-called coexistence method, which consists in directly simulating solid and liquid in coexistence. The method requires large simulations cells, typically containing hundreds or even thousands of atoms, and it is therefore very difficult to apply using first-principles methods, though this has been achieved recently for Al,[12] MgO,[13] LiH,[24] and hydrogen.[25] A third approach, which may be seen as a combination of the two above, consists in fitting an empirical potential to first-principles calculations, obtaining the melting curve of the empirical potential using the coexistence method, and then correcting for the difference between the *ab initio* and the empirical potentials. This approach, which has been described in detail elsewhere,[26] is the one that we adopted in the present work. As we show later, our results are in good agreement with DAC experiments at low pressure but differ from them significantly as pressure is increased, and at high pressure agree well with shock-wave experiments.

The paper is organized as follows. In the next section we report the main technical details used in this work. In Sec. III, tests of the reliability of the techniques and the static equation of state are discussed, whereas lattice dynamics and the thermal equation of state are presented in Secs. IV and V, respectively. The melting curve of tantalum is presented in Sec. VI. Finally, discussion and conclusions are given in Sec. VII.

II. TECHNICAL DETAILS

Calculations have been performed within the framework of density functional theory, using the *ab initio* total-energy and molecular dynamics program VASP,[27–30] with the implementation of an efficient extrapolation for the electronic charge density.[31] The ion-electron interaction has been described using the projector augmented wave (PAW) technique,[32,33] with single-particle orbitals expanded in plane waves with a cutoff of 224 eV, which ensures convergence of the structural parameters of Ta, like the equilibrium volume and the bulk modulus, to better than 0.05%. We tested different exchange-correlation functionals and various PAW potentials, the details of which will be reported in the next section. Spin-orbit effects have also been tested. Thermal excitations of electrons are important at high temperature; we therefore used the finite-temperature formulation of DFT, in which the variational quantity to be minimized is the free energy of the electrons, $F_{static}(V,T)=E(V,T)-TS(V,T)$, where the DFT energy E is the usual sum of kinetic, electron-nucleus, Hartree, and exchange-correlation terms, and S is the electronic entropy, given by the independent-electron formula $S=-k_B T\Sigma_i[f_i \ln f_i+(1-f_i)\ln(1-f_i)]$, with k_B being the Boltzmann constant and f_i the thermal (Fermi-Dirac) occupation number of orbital i. Brillouin zone (BZ) sampling was performed using Monkhorst-Pack (MP) special points.[34] Constant temperature molecular dynamics simulations were performed using a Nosé thermostat,[35] with a time step of 2 fs.

III. EQUATION OF STATE

The Helmholtz free energy of a solid can be written as a sum of two different contributions:

$$F(V,T) = F_{static}(V,T) + F_{vib}(V,T), \tag{1}$$

where $F_{static}(V,T)=E(V,T)-TS(V,T)$ is the zero-temperature energy plus the contribution arising from thermal electronic excitation in the perfect crystal, and $F_{vib}(V,T)=F_{harm}(V,T)+F_{anharm}(V,T)$ is the contribution due to the vibrations of the ions, written as a sum of harmonic and anharmonic contributions. $F_{static}(V,T)$ can be obtained as a result of a standard DFT calculation. The treatment of the ionic component of the free energy $F_{vib}(V,T)$, neglecting the anharmonic contribution in all the calculations, will be described in the next section.

Within the plane wave formalism of DFT with PAW potentials we tested the local density approximation (LDA) and the generalized gradient approximations (GGAs) known as the Perdew-Burke-Ernzerhof[36] (PBE) and the Perdew-Wang 1991 (Ref. 37) (PW91) functionals. We found negligible differences between the PW91 and the PBE results, and therefore in what follows we will only report results obtained using the LDA and the PBE functionals. We calculated the total electronic static (free) energy for different volumes on the perfect Ta bcc crystal, and fitted the calculated (free) energies to the third-order Birch-Murnaghan equation[38–40]

$$F_{static}(V) = E_0 + \frac{3}{2}V_0K_0\left[-\frac{\chi}{2}\left(\frac{V_0}{V}\right)^2 + \frac{3}{4}(1+2\chi)\left(\frac{V_0}{V}\right)^{(4/3)} - \frac{3}{2}(1+\chi)\left(\frac{V_0}{V}\right)^{(2/3)} + \frac{1}{2}\left(\chi+\frac{3}{2}\right)\right], \tag{2}$$

where E_0 and $K_0=-V_0 d^2F_{static}/dV^2$ are the values of the energy and the bulk modulus at equilibrium volume V_0, respectively, $\chi=\frac{3}{4}(4-K_0')$, and $K_0'=[\partial K/\partial P]$, with the derivative evaluated at zero pressure. The static equation of state ($P-V$ curve) is obtained as the derivative of Eq. (2) as a function of the volume.

In all calculations we used an electronic temperature of $T=300$ K, and we found that with a $16\times16\times16$ MP grid of **k** points the electronic free energy of the bcc primitive cell was converged to within less than 1 meV.

We tested PAW potentials with the $5p$ electrons either frozen in the core, or explicitly included in valence, together with the $6s$ and $5d$ electrons. In Fig. 1 we display the results of the calculations using the two different PAW potentials, both with PBE and LDA, compared with the diamond anvil cell experiments from Refs. 41–43. We see, that in order to obtain good accuracy it is necessary to use the functional PBE and the PAW potentials which explicitly include the $5p$ electrons in the valence. These results agree well also with a number of previous calculations.[9,44]

We also tested spin-obit(SO) coupling, with both the LDA and the GGA. With the LDA we found an increase of about 0.3% in the equilibrium volumes when spin-orbit coupling is switched on, and with the GGA the results are almost identical. These small effects are in agreement with previous calculations done by Bercegeay and Bernard,[8] Boettger *et al.*,[45] and Cohen and Gülseren,[44] though at variance with previous full potential linear muffin-tin orbital results by Söderlind and Moriarty,[46] who found a significant spin-orbit effect on the equilibrium volume, which decreases by about 3% when

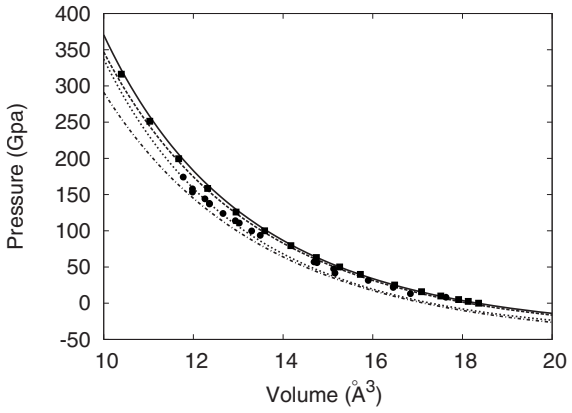

FIG. 1. Pressure vs volume curves obtained by fitting a Birch-Murnaghan equation of state to DFT calculated values for bcc Ta. Curves show results obtained using the LDA with (points) and without (points and dashed line) the inclusion of 5*p* electrons in valence. The same calculations using the PBE functional with (solid) and without (dashed) the inclusion of 5*p* electrons in valence. Diamond anvil cell data from Refs. 41 (squares) and 43 (solid circles) are also reported for comparison.

spin-orbit coupling was switched on. Table I summarizes the final values of the parameters at zero pressure obtained in the present work as compared to the DAC data obtained by Cynn and Yoo.[41]

After these tests, we decided to use the PBE functional in all calculations, the PAW potential with 5*p* electrons in valence, and to neglect spin-orbit interactions.

IV. LATTICE DYNAMICS

To further test the quality of the PAW potential and the PBE exchange-correlation functional to be employed in this work, we also calculated phonon dispersion relations, both at zero and at high pressure. These have been calculated using the PHON code[47] which implements the small displacement method described in Refs. 22 and 48. Within this method, the quantity that is directly calculated is the force-constant matrix $\Phi_{\alpha,\beta}(\mathbf{R})$, where $\mathbf{R}$ is the position of the ions in the crystal and α,β indicate Cartesian coordinates. This can be evaluated by displacing the atom in one primitive cell by a small amount, and computing the forces induced on all the other atoms in the system. The force-constant matrix is then simply the constant of proportionality between the displacement and the forces. The phonon frequencies $\omega_{\mathbf{q}s}$ for any $\mathbf{q}$ vector in the BZ and any branch s are obtained as eigenvalues of the dynamical matrix, which is given by

$$D_{\alpha,\beta}(\mathbf{q}) = \frac{1}{\sqrt{M}} \sum_{\mathbf{R}} \Phi_{\alpha,\beta}(\mathbf{R}) \exp(i\mathbf{q}\cdot\mathbf{R}), \tag{3}$$

where M is the mass of the tantalum atom and the sum has to be evaluated for every lattice vector $\mathbf{R}$ in the crystal. In fact, $\Phi(\mathbf{R})$ is usually short ranged, and therefore one only needs to include in the sum those terms for which $\Phi(\mathbf{R})$ is appreciably different from zero. This makes the small displacement method feasible, as one only needs $\Phi(\mathbf{R})$ in a finite supercell. Convergence of the phonon frequencies $\omega_{\mathbf{q}s}$ is then ensured by progressively increasing the size of the supercell used to evaluate $\Phi(\mathbf{R})$.

The force-constant matrix, and therefore the phonon frequencies, can depend on temperature because of electronic excitations. In this work we neglected this dependence.

We tested the convergence of the phonon frequencies with respect to a number of technical points. The quantity used to measure the quality of the results was the ionic free energy in the quasiharmonic approximation, given by

$$F_{harm}(V,T) = \frac{1}{N_{\mathbf{q}}} k_B T \sum_{\mathbf{q},s} \ln\left[2\sinh\left(\frac{\hbar\omega_{\mathbf{q}s}(V)}{2k_{\mathrm{B}}T}\right)\right], \tag{4}$$

where the sums are over phonon wave vectors $\mathbf{q}$ in the BZ and branches s, and $N_{\mathbf{q}}$ is the number of $\mathbf{q}$ points in the sum. First, we tested the size of the displacement, which has to be small in order to be in the validity range of the harmonic approximation, but also big enough so that the forces induced in the crystal are not too small compared to the numerical noise in the calculations. We found that a value of 0.02 Å is a good compromise, and allows us to obtain free energies at 300 K converged within 1 meV. The calculations were done using a $2\times2\times2$ supercell (eight atoms). Second, we tested convergence with respect to $\mathbf{k}$-point sampling, and we found that an $8\times8\times8$ MP $\mathbf{k}$-point grid is necessary to obtain a free energy converged within 1 meV at 300 K. Third, we tested the size of the supercell, performing calculations with up to $8\times8\times8$ supercells (512 atoms), and found that the convergence of the free energy was obtained using cells containing at least 64 atoms ($4\times4\times4$). With a 512-atom supercell, the only Γ-point sampling of the BZ has been calculated. Finally, we did convergence tests on the grid of $\mathbf{q}$ points in which the phonons are calculated, and found that with a $24\times24\times24$ $\mathbf{q}$-point grid the quasiharmonic free energy is converged to 1 meV.

In Fig. 2 we plot the dispersion curves at zero pressure along several high-symmetry directions in the Brillouin zone for both transverse (TA) and longitudinal (LA) acoustical branches obtained using the 512-atom supercell. An almost

TABLE I. Zero-pressure equilibrium volume V_0 and bulk modulus K_0 for bcc Ta in comparison with DAC data from Ref. 41. All values obtained using the PAW potential with the 5*p* electrons explicitly included in valence.

	LDA	LDA+SO	PBE	PBE+SO	DAC data
V_0 (Å^3)	17.23	17.28	17.91	17.90	18.04
K_0 (GPa)	214	212	197	197	194

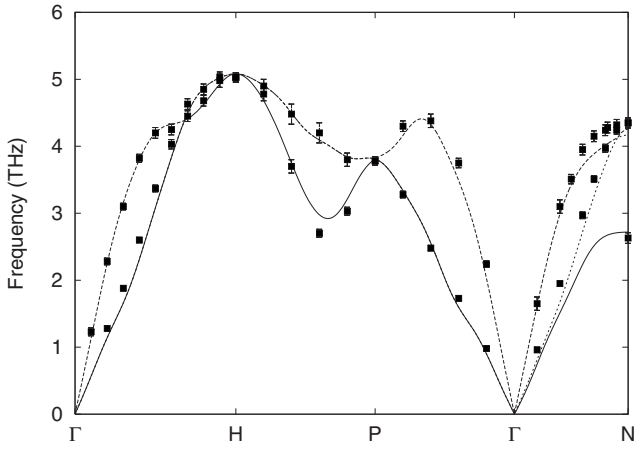

FIG. 2. Phonon dispersion curves at zero pressure for bcc Ta. Squares with error bars are neutron diffraction experiments (Ref. 49).

perfect agreement is obtained in comparison to the inelastic neutron diffraction data by Woods[49] and previous theoretical calculations by Bercegeay *et al.*[8] The calculations have been repeated for 20 further different volumes using only 64-atom cells, which show no significant degradation of the phonon dispersion curves. As expected, the results show the well-known phenomenon in solids of increasing phonon frequencies with decreasing volume (increasing pressure), which is responsible for the positive thermal expansion. Figure 3 shows some of the dispersion curves corresponding to pressures from 6 to 325 GPa.

V. HIGH-TEMPERATURE EQUATION OF STATE

Previous calculations on tantalum[8,44] suggest that the total free energy, i.e., the electronic free energy term plus the vibrational contribution, can be fitted to the Vinet equation of state for each temperature T. Here we took a similar approach. We calculated the static and the vibrational parts of the free energy at a number of different temperatures between 293 and 6500 K, and for each temperature fitted the total free energy to a third-order Birch-Murnaghan equation of state. We obtained a set of parameters $V_0(T)$, $K_0(T)$, $E_0(T)$, and $K_0'(T)$, which we report in Table II for some values of T. The temperature dependence of these quantities has been further parametrized using third-order spline functions in T. Figure 4 shows the Birch-Murnaghan parameters $E_0(T)$, $V_0(T)$, $K_0(T)$ as functions of temperature. Previously calculated values from Ref. 44, where the parameters were fitted using the Vinet equation of state, are in good agreement with the present work.

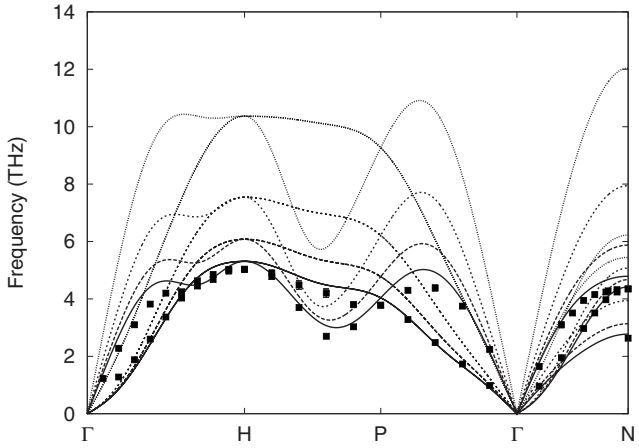

FIG. 3. Phonon dispersion curves calculated at pressures of 6 (solid line), 28 (dashed line), 95 (short dashed line), and 325 (dotted line) GPa.

TABLE II. Birch-Murnaghan fitted parameters for bulk bcc Ta as a function of temperature.

T (K)	$E_0(T)$ (eV)	$V_0(T)$ (Å^3)	$K_0(T)$ (GPa)
293	−11.728	18.34	186
1174	−12.327	18.69	173
2113	−13.197	19.13	157
3052	−14.218	19.79	137
4226	−15.646	20.44	121
5166	−16.898	21.24	104
6105	−18.218	21.85	87
6574	−18.871	22.10	80

Figure 5 shows the room temperature thermal pressure (defined as the total pressure minus the static pressure) as a function of volume. Our calculations indicate, in agreement with Cohen and Gülseren,[44] that the thermal pressure contribution is very small in the whole pressure range ~0–300 GPa, being less than 1 GPa at low pressure and increasing only to about 2 GPa at high pressure.

A very important parameter for the interpretation of shock experiments is the Grüneisen parameter defined by

$$\gamma = V\left(\frac{\partial P}{\partial E}\right)_V = \frac{\alpha K_T V}{C_V}, \tag{5}$$

where E is the internal energy and α, K_T, and C_V are the thermal expansivity, isothermal bulk modulus, and constant volume specific heat, respectively. Figures 6 and 7 show the

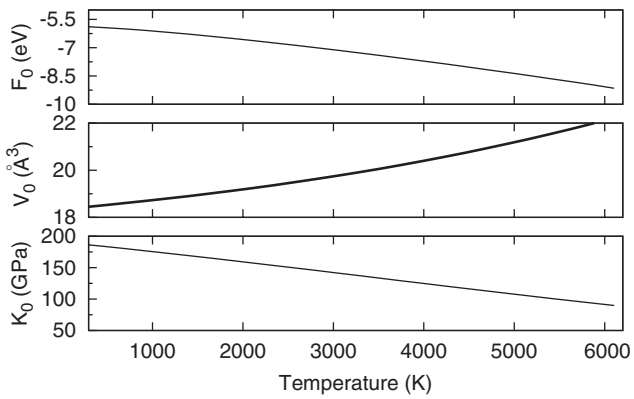

FIG. 4. Birch-Murnaghan parameters as a function of the temperature. (a) Minimum energy $F_0(T)$, (b) $V_0(T)$, and (c) $K_0(T)$.

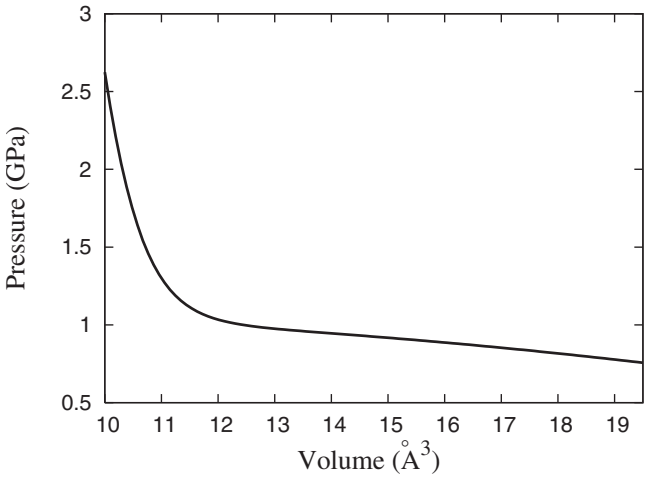

FIG. 5. Thermal pressure at room temperature as a function of volume.

variation of the Grüneisen parameter as a function of temperature and pressure, respectively. We found a smooth variation of the Grüneisen parameter with temperature in the range of pressures considered, and a large increase for pressures below 100 GPa. Our results are similar to those reported by Cohen and Gülseren,[44] but they predict a more pronounced variation with pressure than those of Bercegeay and Bernard[8] and those of Moriarty *et al.*[3] The experimental zero-pressure room temperature value of the Grüneisen parameter is 1.65, which agrees well with the calculations of Bercegeay and Bernard[8] and, to some extent, those of Moriarty *et al.*[3] (who only reported the ionic contribution), but is lower than that found in the present calculations (and those of Cohen and Gülseren[44]).

VI. MELTING CURVE OF TANTALUM

To calculate the melting curve of Ta we applied the method of the coexistence of phases plus free energy corrections, as described earlier.[26] The strategy can be summarized in the following three steps. The first step is to find a good reference potential that mimics as closely as possible the *ab initio* system. The second is to use this reference potential to compute the melting temperature at a chosen pressure. This is done by performing simulations in large boxes in which solid and liquid are simulated at the same time. If simulations are performed in the *NVE* ensemble, then for any choice of volume V there exists a range of internal energy E for which solid and liquid coexist for long time. The average pressure and temperature over the coexisting period then provide a point on the melting curve of the reference potential. We will describe this in more detail below. The third and final step is the evaluation of the difference in melting temperature between the reference system and the *ab initio* one. This evaluation is repeated at various pressures on the reference model melting curve in order to produce the DFT melting curve. As shown earlier,[26] for a chosen pressure p the difference in melting temperature between the reference potential and the *ab initio* system is given, to first order, by

$$T_m' = \Delta G^{ls}(T_m^{\text{ref}})/S_{\text{ref}}^{ls}, \tag{6}$$

where $\Delta G^{ls}(T_m^{\text{ref}})$ is the difference in the Gibbs free energies between the *ab initio* system and the reference potential, evaluated at the melting temperature of the reference potential T_m^{ref}, and the superscript *ls* indicates the difference between solid and liquid. S_{re}^{ls} is the entropy of melting of the reference potential, and it is readily evaluated. If the differences in the Gibbs free energies between the *ab initio* system and the reference potential are not too large they can be evaluated using a perturbational approach to thermodynamic integration:

$$\Delta G(p,T) = \langle \Delta U \rangle_{\text{ref}} - \frac{1}{2}\beta \langle \delta \Delta U^2 \rangle_{\text{ref}} + \cdots, \tag{7}$$

where $\beta = 1/k_B T$, $\langle \cdot \rangle_{\text{ref}}$ indicates the thermal average evaluated in the reference potential ensemble, $\Delta U = U - U_{\text{ref}}$, with

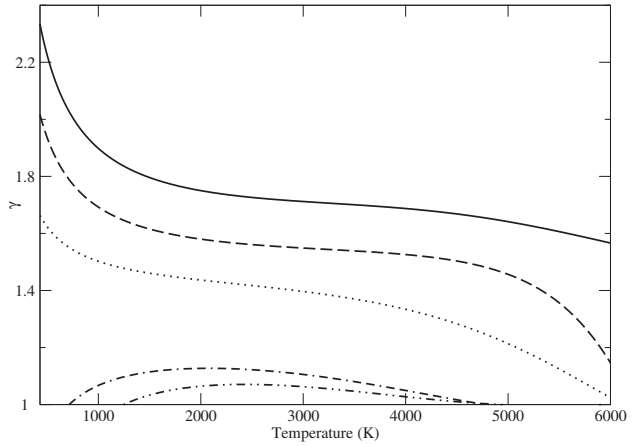

FIG. 6. Variation of the Grüneisen parameter with temperature. Different line styles correspond to different isobars: solid line (0 GPa), dashed line (50 GPa), dotted line (100 GPa), dot-dashed line (200 GPa), and double-dot-dashed line (300 GPa).

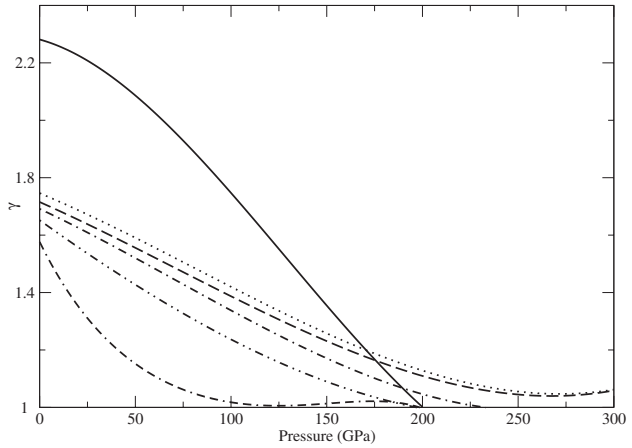

FIG. 7. Variation of the Grüneisen parameter on pressure. Different line styles correspond to different isotherms: solid line (300 K), dotted line (2000 K), dashed line (3000 K), dot-dashed line (4000 K), double-dot point dashed (5000 K), double-dash-dotted line (6000 K).

U and U_{ref} the *ab initio* and the reference potential total energy functions, respectively, and $\delta\Delta U=\Delta U-\langle\Delta U\rangle_{\mathrm{ref}}$. We prefer to work with the isothermal-isochoric ensemble, and we therefore evaluate the difference in the Helmholtz free energies $\Delta F(V,T)$,

$$\Delta F(V,T)=\langle\Delta U\rangle_{\mathrm{ref}}-\frac{1}{2}\beta\langle\delta\Delta U^2\rangle_{\mathrm{ref}}+\cdots. \tag{8}$$

Then, the relation between ΔG and ΔF is readily shown to be

$$\Delta G=\Delta F-\frac{1}{2}V\kappa_T\Delta p^2+o(\Delta p^3), \tag{9}$$

where Δp is the difference in pressure as the potential energy function is changed from the reference potential to the *ab initio* system at constant volume V, κ_T is the isothermal compressibility, and ΔG is obtained at the pressure p of the reference system at volume V.

The reference potential used in the present calculation is an embedded atom model[50] in which the total energy is given by

$$E_{\mathrm{tot}}=\frac{1}{2}\epsilon\sum_{i\neq j}\left(\frac{a}{r_{ij}}\right)^n-\epsilon C\sum_i\left[\sum_{j(\neq i)}\left(\frac{a}{r_{ij}}\right)^m\right]^{1/2}. \tag{10}$$

where r_{ij} is the interatomic separation.

It is clear from Eq. (6) that, in order for the first-order correction to the melting temperature T_m' to be reliable, the difference in Gibbs free energy $\Delta G^{ls}(T_m^{\mathrm{ref}})$ between the DFT and the reference system has to be as small as possible. Moreover, in order for the perturbational approach described in Eq. (8) to be valid it is necessary for the term $\langle\delta\Delta U^2\rangle_{\mathrm{ref}}$ to be small. This requirement provides a natural recipe for fitting the reference potential to the DFT system: the parameters of the EAM are chosen so as to minimize the fluctuations in the energy differences between the EAM and DFT.

Initially, the parameters of the potential were fitted to a DFT simulation of liquid Ta performed near zero pressure and at a temperature of 3500 K, which gave $n=5.734$, $m=3.462$, $\epsilon=0.743$, $a=3.222$, and $C=6.601$. With this potential we then performed a first series of coexistence simulations in the following way. We constructed a large box by periodically repeating the bcc crystal, represented in a simple cubic box, eight times in the x and y directions and 16 times in the z direction, to obtain a rectangular-shaped supercell containing 2048 atoms. The system was then thermalized to a guessed melting temperature T_{guess}, by simulating for 10 ps in the (NVT) ensemble. Then we raised the temperature to a very large value, keeping the atoms in the left half of the simulation box fixed. Once melting in the right half of the cell occurred, we rethermalized the system back to T_{guess}, with the atoms in the left half of the box still fixed. Then we released the atoms in the left half of the box and let the simulation continue in the (NVE) ensemble. If the amount of total energy E present in the system is chosen appropriately, solid and liquid coexist for a long time, and the averages of the pressure p and temperature T during the simulation provide a point on the melting curve. For every fixed volume V there is a range of values of E which realize this condition. Of course, the initial choice of E (which in our case is tuned by assigning initial velocities to the atoms at the beginning of the simulation) rarely falls into this range, and the system completely melts (solidifies), if E is too large (small), so a number of trial and error steps are necessary before a right choice of E is made.

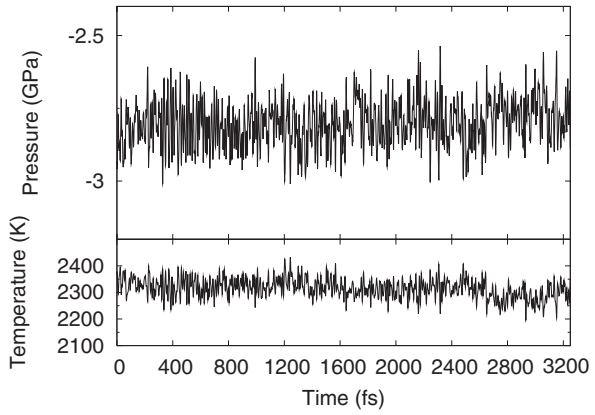

FIG. 8. Time variation of pressure (upper figure) and temperature (lower figure) during a coexistence simulation of solid and liquid Ta at low pressure.

To monitor the simulations we used a number of tools, including the mean square displacement and, in particular, the planar density, defined as the number of atoms present in a slice of the simulation box cut parallel to the solid-liquid interface: in the solid region this planar density is a periodic function, being large when the slice contains a plane of atoms and small when it falls in between planes, while in the liquid region it is simply a random number fluctuating around an average value.

This first series of coexistence simulations were performed to obtain a point on the melting curve near zero pressure. The temperature and pressure calculated throughout this simulation are displayed in Fig. 8, from which we extracted the values $p=-2.8$ GPa and $T=2320$ K. In Fig. 9 we show a snapshot of the density profile which clearly indicates solid and liquid in coexistence. We tested size effects on

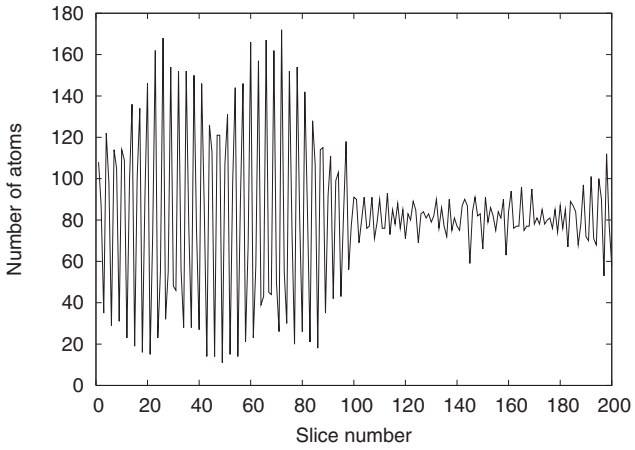

FIG. 9. Snapshot of the density profile during a coexistence simulation of solid and liquid Ta.

TABLE III. Thermal averages $\langle \Delta U \rangle$ and fluctuations $\langle \delta \Delta U \rangle$ (see text for definition) for different sizes of the supercell at $p=-2.8$ GPa and $T=2320$ K for solid and liquid Ta. Calculations have been performed using the Γ point only (Γ). Tests carried out using four **k** points with a 128-atom cell and by averaging in the *ab-initio* ensemble (AI) are also reported. Values are in eV and errors on the last decimal digit.

	$\langle \Delta U \rangle / N$		$-\frac{1}{2}\beta \langle \delta \Delta U^2 \rangle / N$	
N	Liquid	Solid	Liquid	Solid
128 (Γ)	2.733(2)	2.688(2)	−0.026(9)	−0.027(7)
216 (Γ)	2.732(1)	2.708(2)	−0.008(4)	−0.021(7)
250 (Γ)	2.729(2)	2.708(2)	−0.017(8)	−0.021(7)
128 (4**k**)	2.729(2)	2.708(3)	−0.001(1)	−0.013(4)
128 (AI)	−2.666(1)	−2.625(1)	−0.037(3)	−0.035(1)

these results by repeating the simulations using a 16 384-atom cell, which showed essentially identical results.

To compute the DFT corrections to the EAM melting curve we therefore applied Eqs. (6), (8), and (9) above. This has been done in the following way. For a chosen (p, T_m^{EAM}) point on the melting curve of the EAM potential we performed long simulations in the EAM ensemble with $T = T_m^{\mathrm{EAM}}$, and adjusted the volume V separately in solid and liquid in order to obtain p as the average pressure. We then extracted typically 50 statistically independent configurations and calculated the *ab initio* total energies and pressures on these configurations. We separately tested size and **k**-point effects by performing simulations on 128, 216, and 250 atoms with the Γ point only, and then repeating the calculations on the 128-atom systems using four **k** points. The results of these tests are summarized in Table III, where we report the quantities $\langle \Delta U \rangle_{\mathrm{EAM}}$ and $-\frac{1}{2}\beta \langle \delta \Delta U^2 \rangle_{\mathrm{EAM}}$. We notice that all results are very close, with only a small difference of about 20 meV/atom in the results for the solid for $\langle \Delta U \rangle_{\mathrm{EAM}}$ in the calculations performed with the 128-atom cell and the Γ point. We then decided to perform all calculations using the Γ point only and simulation cells containing 250 atoms. We also tested the reliability of the perturbative approach to obtain ΔF using Eq. (8) by repeating the calculations in the *ab initio* ensemble, i.e., by evaluating

$$-\Delta F(V,T) = \langle -\Delta U \rangle_{\mathrm{AI}} + \frac{1}{2}\beta \langle \delta \Delta U^2 \rangle_{\mathrm{AI}} + \cdots , \qquad (11)$$

where now $\langle \cdot \rangle_{\mathrm{AI}}$ indicates the thermal average evaluated in the *ab initio* ensemble. The simulations have been performed with 128-atom cells, and only with Γ-point sampling, and are also reported in Table III. We notice that the term $-\frac{1}{2}\beta \langle \delta \Delta U^2 \rangle_{\mathrm{AI}}$ is slightly larger in this case; however, when summed to the $\langle \Delta U \rangle_{\mathrm{AI}}$ term the results for ΔF are equal to those obtained in the EAM ensemble to within 5 meV/atom.

We then calculated the full melting curve of this EAM potential, and computed the free energy differences between the model and the *ab initio* system at a number of points on the melting curve. Unfortunately, we found that the quality of the EAM potential fitted at low pressure was not good enough to obtain reliable corrections also in the high-pressure region, and we therefore refitted a second EAM potential on a solid simulation performed at $p=49.7$ GPa and $T=4310$ K. We obtained slightly different parameters, given by $n=5.471$, $m=3.317$, $\epsilon=0.353$, $a=3.898$, and $C=14.23$, and we found that this potential could be used in the whole range of pressures 0–300 GPa. The melting curve obtained using this EAM potential and the *ab initio* one obtained by adding on corrections according to Eqs. (6), (8), and (9) are displayed in Fig. 10, where we compare our results with the available DAC and shock-wave experiments and previous theoretical results by Moriarty *et al.*[3] and Strachan *et al.*[19] The calculated values are given in Table IV. The interpolated value of the melting temperature at zero pressure ($T_m = 3270$ K) is in good agreement with DAC experiments[7] ($T_m = 3270$ K), but as the pressure is increased the agreement with DAC experiments quickly deteriorates, and at ~100 GPa the difference between our DFT calculations and

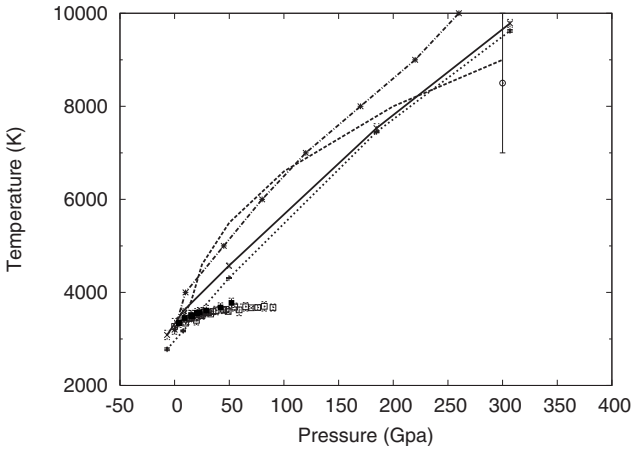

FIG. 10. Phase diagram of Ta obtained using the EAM and the coexistence molecular dynamics MD approach (dotted line), and the resulting *ab initio* curve obtained after adding free energy corrections (solid line). Also reported are DAC melting (Ref. 7) (crosses and open squares), shock melting (Ref. 5) (open circle), and calculations from Ref. 3 (dot-dashed line) and Ref. 19 (dashed line).

TABLE IV. Melting temperature T_m^{EAM} of the EAM at various pressures and *ab initio* corrections T'_m (see text).

P (GPa)	T_m^{EAM} (K)	T'_m (K)
−6.9	2778±30	307±100
7.8	3103±20	495±65
49.7	4310±10	264±55
184.7	7450±20	80±96
306.8	9620±30	50±85

these DAC experiments is already about 2000 K. At 307 GPa our calculated value T_m=9783±85 K is in good agreement within the statistical error bars with shock-wave experiments,[5] which estimate T_m=8500±1500 K.

VII. DISCUSSION AND CONCLUSIONS

The main result of this work is the *ab initio* calculation of the melting curve of Ta, performed with the DFT GGA and PAW potentials. This has been evaluated by combining coexistence calculations based on an interatomic embedded atom model (a reference potential), and DFT corrections. Since the method relies on a perturbative approach to evaluate the corrections between the reference potential melting curve and the DFT one, it is imperative that the reference potential accurately mimics the DFT one. There are two main requirements here: the first is that the energy fluctuations in the energy differences between the reference model and the DFT one must be small, and the second is that the average energy differences between the model and the DFT system must be the same, or as close as possible, in both solid and liquid. To satisfy both requirements may not be easy, and indeed we found that our first fit performed at nearly zero pressure was not good enough in the high-pressure region, and we needed to refit the model potential at an intermediate pressure. We used this potential in the whole pressure region because this second potential seemed to perform well everywhere, but we note that there is no reason why one should use the same potential at each pressure.

The calculated melting curve is in good agreement with DAC experiments in the very low-pressure regime, but starts to differ with increasing pressure. At high pressure our calculated melting curve disagrees substantially with DAC experiments, but is in good agreement with shock data at 300 GPa. Our results on melting are comparable with previous calculations obtained using empirical potentials, though our melting curve is somewhat lower.

The reliability of the calculations is supported by the investigation of a number of thermodynamic properties of tantalum. We have calculated the equation of state (P-V curves) with different correlation-exchange functionals and found essential the use of a PBE functional and PAW potentials, which explicitly treat as valence electrons the 5p, 6s, and 5d electrons. A very good agreement for the equation of state has been found with the most recent DAC data on tantalum,[43] which differ somewhat from previous experimental measurements.[41] Of course, a fair comparison should include thermal expansion effects at room temperature, where the experiments have been performed, however our calculations show that the thermal pressure is only a very small contribution at room temperature, being less than 1 GPa at low pressure and increasing only to about 2 GPa at high pressure. We have found that the contribution of spin-orbit coupling has negligible effects in the calculation of the equation of state. We also performed lattice dynamics calculations using the small displacement method, obtaining almost perfect agreement of phonon dispersion curve at zero pressure with neutron diffraction measurements. Within the quasiharmonic approximation, we studied finite-temperature properties, and in particular we calculated the Grüneisen parameter, which is used together with the constant volume specific heat (not reported here) to calculate temperatures on the Hugoniot in shock-wave experiments. We found that the Grüneisen parameter depends weakly on temperature in the range of pressures investigated (0–300 GPa), but has a stronger dependence on pressure in the range of temperature 300–6000 K. These findings agree well with those previously reported by Cohen and Gülseren.[44] The pressure variation of the Grüneisen parameter is also in agreement with the results of Cohen and Gülseren,[44] and it is more pronounced than that found by Bercegeay and Bernard[8] and by Moriarty *et al.*[3] Our calculated zero-pressure room temperature value of the Grüneisen parameter is just over 2.0, which is higher than the experimental value, equal to 1.65. We have not considered anharmonic effects in these calculations, but we do not believe that they would change significantly the value of the Grüneisen parameter. Anharmonic effects were investigated in our previous work on hcp Fe,[22] where we found a very small anharmonic contribution (at high temperature) to the specific heat and the thermal pressure. These small contributions also had the same sign, and therefore partially cancel when used in the evaluation of the Grüneisen parameter.

These results *per se* do not shed light on the reasons for the large disagreement between DAC melting curves of transition metals on one side, and first-principles calculations (generally in agreement with shock data experiments) on the other, but provide additional data substantiating these differences. There seems to be a consistent pattern of disagreement between *ab initio* and DAC melting of transition metals, as this disagreement is observed also in Mo and Fe (although recent DAC experiments[18] on Fe show good agreement with the *ab initio* calculations[15]). The disagreement with the DAC experiments is large enough to cause concern, and it is difficult to comment on why this is. We believe that at least some of the DAC experiments may suffer from an imperfect diagnostic tool to detect melting, like the use of the intensity of x-ray diffraction peaks,[6] which might lead to underestimating the melting temperature. Another possible problem in DAC experiments is the temperature measurement. Recently, an analysis of the spectroradiometrics effects of the dispersion and adsorbance properties of diamond has found that chromatic effects induced by the diamond windows can be substantial, and may lead to an underestimate of melting temperatures of several hundred degrees.[51] Applying this analysis to the melting curve of Benedetti *et al.*[51] concluded that, for example, the melting curve of Boehler[16] and that of Saxena and Dubrovinski[52] are at least a few hundred degrees

too low at megabar pressures. On the theoretical side we cannot exclude the possibility that density functional theory may be in error, although this is difficult to believe given the large quantity of experimental data accurately predicted by this level of theory. Nevertheless, it has been shown that in some cases different approximations for the exchange-correlation functional do indeed result in different melting temperatures. For example, in both MgO (Ref. 13) and Al (Refs. 11 and 12) the GGA gives a zero-pressure melting temperature that is about 20% lower than the experimental one, while the LDA provides a melting temperature in very good agreement with the experiments, although this difference between the two is progressively removed as pressure is increased. Silicon is another example where the LDA and GGA give different answers, though in this case it is the LDA that underestimates the melting temperature.[21,53] This would leave scope for going beyond the DFT to try to improve on the accuracy of *ab initio* calculations. For Ta the difference between the calculations and the experiments is very large, and we believe that it is very unlikely for DFT to be so much in error.

ACKNOWLEDGMENTS

This work was supported by NERC Grant No. NE/C51889X/1 and by EPSRC Grant No. EP/C534360, which is 50% funded by DSTL (MOD). We also acknowledge support from EPSRC through a EURYI grant (D.A.). Allocation of computer time on the HPCx service was provided by NERC, and on the UCL facilities by Research Computing.

[1] N. W. Ashcroft and D. A. Mermin, *Solid State Physics* (HRW International Editions, New York, 1976).
[2] A. Jiang, T. A. Tyson, and L. Axe, J. Phys.: Condens. Matter **17**, 1841 (2005).
[3] J. A. Moriarty, J. F. Belak, R. E. Rudd, P. Söderlind, F. H. Streitz, and L. H. Yang, J. Phys.: Condens. Matter **14**, 2825 (2002).
[4] A. C. Mitchell and W. J. Nellis, J. Appl. Phys. **52**, 3363 (1981).
[5] J. M. Brown and J. W. Shaner, in *Shock Waves in Condensed Matter*, edited by J. R. Asay *et al.* (Elsevier, New York, 1984).
[6] D. Errandonea, M. Somayazulu, D. Häusermann, and D. Mao, J. Phys.: Condens. Matter **15**, 7635 (2003).
[7] D. Errandonea, B. Schwager, R. Ditz, C. Gessmann, R. Boehler, and M. Ross, Phys. Rev. B **63**, 132104 (2001).
[8] C. Bercegeay and S. Bernard, Phys. Rev. B **72**, 214101 (2005).
[9] Y. Wang, D. Chen, and X. Zhang, Phys. Rev. Lett. **84**, 3220 (2000).
[10] G. A. de Wijs, G. Kresse, and M. J. Gillan, Phys. Rev. B **57**, 8223 (1998).
[11] L. Vočadlo and D. Alfè, Phys. Rev. B **65**, 214105 (2002).
[12] D. Alfè, Phys. Rev. B **68**, 064423 (2003).
[13] D. Alfè, Phys. Rev. Lett. **94**, 235701 (2005).
[14] D. Alfè, M. J. Gillan, and G. D. Price, Nature (London) **401**, 462 (1999).
[15] D. Alfè, G. D. Price, and M. J. Gillan, Phys. Rev. B **65**, 165118 (2002).
[16] R. Boehler, Nature (London) **363**, 534 (1993).
[17] G. Shen, H. Mao, R. J. Hemley, T. S. Duffy, and M. L. Rivers, Geophys. Res. Lett. **25**, 373 (1998).
[18] Y. Ma, G. Somayazulu, G. Shen, H. K. Mao, J. Shu, and R. J. Hemley, Phys. Earth Planet. Inter. **143-144**, 455 (2004).
[19] A. Strachan, T. Çağin, O. Gülseren, S. Mukherjee, R. E. Cohen, and W. A. Goddard III, Modell. Simul. Mater. Sci. Eng. **12**, 445 (2004).
[20] D. Errandonea, Physica B **357**, 356 (2005).
[21] O. Sugino and R. Car, Phys. Rev. Lett. **74**, 1823 (1995).
[22] D. Alfè, G. D. Price, and M. J. Gillan, Phys. Rev. B **64**, 045123 (2001).
[23] D. Alfè, G. D. Price, and M. J. Gillan, Phys. Rev. B **64**, 045123 (2001).
[24] T. Ogitsu, E. Schwegler, F. Gygi, and G. Galli, Phys. Rev. Lett. **91**, 175502 (2003).
[25] S. A. Bonev, E. Schwegler, T. Ogitsu, and G. Galli, Nature (London) **431**, 669 (2004).
[26] D. Alfè, M. J. Gillan, and G. D. Price, J. Chem. Phys. **116**, 6170 (2002).
[27] G. Kresse and J. Hafner, Phys. Rev. B **47**, 558 (1993).
[28] G. Kresse and J. Hafner, Phys. Rev. B **49**, 14251 (1994).
[29] G. Kresse and J. Furthmüller, Comput. Mater. Sci. **6**, 15 (1996).
[30] G. Kresse and J. Furthmüller, Phys. Rev. B **54**, 11169 (1996).
[31] D. Alfè, Comput. Phys. Commun. **118**, 31 (1999).
[32] P. E. Blöchl, Phys. Rev. B **50**, 17953 (1994).
[33] G. Kresse and D. Joubert, Phys. Rev. B **59**, 1758 (1999).
[34] H. J. Monkhorst and J. D. Pack, Phys. Rev. B **13**, 5188 (1976).
[35] S. Nosé, Mol. Phys. **52**, 255 (1984).
[36] J. P. Perdew, K. Burke, and M. Ernzerhof, Phys. Rev. Lett. **77**, 3865 (1996).
[37] J. P. Perdew, J. A. Chevary, S. H. Vosko, K. A. Jackson, M. R. Pederson, D. J. Singh, and C. Fiolhais, Phys. Rev. B **46**, 6671 (1992).
[38] F. Birch, J. Geophys. Res. **83**, 1257 (1978).
[39] F. Birch, Phys. Rev. **71**, 809 (1947).
[40] F. Murnaghan, Proc. Natl. Acad. Sci. U.S.A. **30**, 244 (1944).
[41] H. Cynn and C. S. Yoo, Phys. Rev. B **59**, 8526 (1999).
[42] M. Hanfland, K. Syassen, and J. Köler, J. Appl. Phys. **91**, 4143 (2002).
[43] A. Dewaele, P. Loubeyre, and M. Mezouar, Phys. Rev. B **70**, 094112 (2004).
[44] R. E. Cohen and O. Gülseren, Phys. Rev. B **63**, 224101 (2001).
[45] J. C. Boettger, Phys. Rev. B **64**, 035103 (2001).
[46] P. Söderlind and J. A. Moriarty, Phys. Rev. B **57**, 10340 (1998).
[47] D. Alfè, computer code PHON (UCL, London, 1998), http://www.chianti.geol.ucl.ac.uk/~dario
[48] G. Kresse, J. Furthmüller, and J. Hafner, Europhys. Lett. **32**, 729 (1995).
[49] A. D. B. Woods, Phys. Rev. **136**, A781 (1964).
[50] M. S. Daw, S. M. Foiles, and M. I. Baskes, Mater. Sci. Rep. **9**, 251 (1993).
[51] L. R. Benedetti, N. Guignot, and D. L. Forber, J. Appl. Phys. **101**, 013109 (2007).
[52] S. K. Saxena and L. S. Dubrovinski, Am. Mineral. **85**, 372 (2000).
[53] D. Alfè and M. J. Gillan, Phys. Rev. B **68**, 205212 (2003).